Overview and Progress Toward High-Efficiency, Air Stable, Cs-Free III-Nitride Photocathode Detectors

Emma Rocco, *Student Member, IEEE*, Jonathan Marini, Kasey Hogan, Vincent Meyers, Benjamin McEwen, L. Douglas Bell, and F. Shahedipour-Sandvik

***Abstract*—We review the recent progress to achieve air stable III-nitride photocathodes for applications as photon detectors. High conductivity *p*-type films are critically important to realize high quantum efficiency (QE) photocathodes with effective negative electron affinity (NEA) and downward surface band bending with narrow surface depletion width. Initial reports of III-nitride photocathodes utilize a Cs-surface activation to achieve effective NEA. To attain air stable, Cs-free photocathodes, novel energy band engineering has been shown using Si delta-doping and an n^+-GaN cap on the surface of a Ga-polar *p*-GaN layer. Improvement of QE has been achieved utilizing the N-polarity of III-nitrides due to advantageous depletion and polarization charges at the surface. High QE $>$ 25% has been demonstrated by improvements in *p*-type conductivity with improved Mg-dopant incorporation in N-polar hillock structures and by control over unintentional impurity incorporation and distribution. Further, the importance of achieving high *p*-type conductivity films is further shown through reviewing recent simulations of GaN photocathodes with varied band bending and hole concentrations. Through comparison of experimental photoemission with Monte Carlo simulations, band structure parameters such as electron effective mass in the conduction band valleys have been elucidated.**

***Index Terms*—III-nitrides, photodetectors, photocathode.**

I. Introduction

III-NITRIDE photodetectors are technologically significant devices, harnessing the wide and tunable band gap of the material system for photon detection of wavelengths spanning from infrared to ultra-violet [1]–[3]. Photocathodes have advantages over other types of photodetectors as they provide low noise and fast response time for single photon detection [4], [5]. Further, the structure of photocathodes is relatively simple, primarily requiring a *p*-type semiconductor, in comparison to detectors such as avalanche photodiodes which require *p-i-n* structures and electrical biasing [6]. Photocathodes are commonly employed in photomultiplier tubes (PMTs) or in arrayed detectors such as microchannel plate (MCP) detectors, and electron bombarded charge coupled device (EBCCD) detectors [2], [7]–[9]. Photocathode-based photodetectors find applications in astronomy for determining the composition of planets and stars, as well as in defense applications for non-line of sight communications and missile detection [9]. Beyond photon detection, photocathodes are utilized as electron sources for ultra-fast electron diffraction and in linear accelerator applications [10]–[12]. Additionally, as electron sources, photocathodes may have the potential for use in electron beam lithography systems [13].

Through the photoemission process, photocathodes absorb incident photons and emit photoexcited electrons. Spicer introduced a three-step model to describe the photoemission process within a bulk material which includes (1) photoexcitation, (2) transport and (3) emission of electrons [14]. The probability of photoemission, *P* as a function of the incident photon angular frequency (ω) and depth from the surface (x) can be described as the product of the individual probabilities of each process, as in (1) [15], [16].

$$P(\hbar\omega) = I_0\alpha_{PE}e^{-\alpha x} \cdot e^{-x/\lambda} \cdot \frac{1}{8}\frac{(\hbar\omega - E_{th})^n}{E_{th}} \quad (1)$$

The probability of photoexcitation is dependent on the incident photon intensity, I_0, and $\alpha_{PE}(\omega)$, a subset of the optical absorption coefficient for photon energies large enough for photoemission, decaying in intensity as a function of depth and the optical absorption coefficient $\alpha(\omega)$. The probability for photoexcited carriers to transport to the surface is exponentially related to the electron scattering length, λ. If a carrier reaches the surface of the photocathode, it must possess sufficient energy to escape the energy barrier, $E_{th,}$ to be emitted into the vacuum level. Here, *n*, is an empirically derived constant – most commonly 2 for metals and 3 for semiconductor materials [17], [18]. By integrating the photoemission probability over an assumed infinite sample depth, the photoemitted electron flux or photocurrent, *J* can be described by:

$$J = \frac{I_0\alpha_{PE}}{\alpha + 1/\lambda}\frac{1}{8}\frac{(\hbar\omega - E_{th})^n}{E_{th}} \quad (2)$$

Manuscript received December 22, 2021; revised February 18, 2022; accepted February 23, 2022. Date of publication March 1, 2022; date of current version March 16, 2022. This work was supported by the National Aeronautics and Space Administration under Grant 80NM0018D0004. *(Corresponding author: Emma Rocco).*

Emma Rocco, Jonathan Marini, Kasey Hogan, Vincent Meyers, Benjamin McEwen, and F. Shahedipour-Sandvik are with the College of Nanoscale Science and Engineering, SUNY Polytechnic Institute, Albany, NY 12203 USA (e-mail: roccoe@sunypoly.edu; jonathan.r.marini@gmail.com; hogank1@sunypoly.edu; meyersv@sunypoly.edu; mcewenb@sunypoly.edu; sshahedipour-sandvik@sunypoly.edu).

L. Douglas Bell is with the Jet Propulsion Laboratory, California Institute of Technology, Pasadena, CA 91109 USA (e-mail: lloyddoug.bell@jpl.nasa.gov).

Digital Object Identifier 10.1109/JPHOT.2022.3155383

As the quantum efficiency is defined as the ratio of photocurrent to incident photons, mathematically QE is described as

$$QE = \frac{\alpha_{PE}}{\alpha + 1/\lambda} \frac{1}{8} \frac{(\hbar\omega - E_{th})^n}{E_{th}} \quad (3)$$

From these equations it can be understood that photocathode quantum efficiency can be improved through two means; (1) decreasing the energy barrier at the surface and (2) reducing scattering events that impede emission. The first can be achieved by the engineering of a favorable energy band alignment compared to the surface vacuum level. In semiconductor photocathodes that rely on a *p*-type absorbing layer, this could be achieved by obtaining a high hole concentration to achieve downward surface band bending with a narrow surface potential well. A small surface depletion width is additionally advantageous toward minimizing detrimental scattering events. As the depletion width narrows, few electrons experience scattering events in this region which may lower the energy below the surface vacuum level and become trapped in the potential well. Surface cleaning to remove contaminants can also be utilized to maximize achievable downward band bending (1) and reduce electron scattering at the surface (2). An ideal photocathode achieves effective negative electron affinity (NEA) where the energy of the conduction band in the bulk is above the vacuum energy level at the surface and therefore there is no energy barrier for emission of electrons photoexcited in the flat-band region. Activation of photocathodes with Cs or Cs/Cs-O coating can achieve such an alignment by lowering of the effective surface vacuum level relative to the bulk, although a thin tunnel barrier remains at the surface [19]. Finally, while phonon scattering is the dominant scattering mechanism, neutral and ionized impurity scattering is possible and thus achieving higher material quality may further decrease carrier scattering and impact QE to a degree [20], [21].

A wide variety of materials have been studied for photocathodes including metals and semiconductors. Among metal photocathodes copper, magnesium, lead, yttrium and niobium are commonly studied, however all suffer from relatively low QE on the order of 10^{-5} to 10^{-3}, and require UV illumination [22]. Commonly used semiconductor photocathodes may be alkali-based or activated III-V crystals [10], [15]. Alkali photocathodes such as Cs_2Te, K_2CsSb, CsI, and KBr exhibit high quantum efficiencies of 10%, 25%, 30% and 50%, respectively [10], [23], [24]. These materials detect photons of energies spanning the visible to UV wavelengths, and the photocathode material can be chosen to match the desired spectral range for a specific application. Alkalis are highly reactive to ambient gases such as O_2, CO, CO_2, and moisture which requires many of these photocathodes to be fabricated, packaged and tested in ultra-high vacuum (UHV) environments, and they are susceptible to degradation over time due to imperfect vacuum and ion back bombardment [25]. Of the alkali photocathodes Cs_2Te retains a relatively long lifetime on the order of months in vacuum [26]. III-V semiconductors, such as $Al_xGa_{1-x}As$ and $Al_xGa_{1-x}N$, are ideal candidates for photocathodes as they have tunable bandgaps through compositional alloying, and effective NEA can be achieved by a thin Cs-activation layer on the surface [27], [28]. Cs-activated III-V photocathodes, similar to alkali materials, degrade due to exposure to ambient gases and require constant presence in vacuum. The III-nitride material system specifically is ideal for use as in photocathodes as it is inherently chemically inert and radiation hard, meaning that devices will experience minimal degradation due to exposure to air, moisture, and high energy radiation. Additionally, by alloying III-nitride materials the theoretical range of detection spans from the infra-red at 1900 nm to deep UV at 200 nm, grading from InN to AlN, respectively.

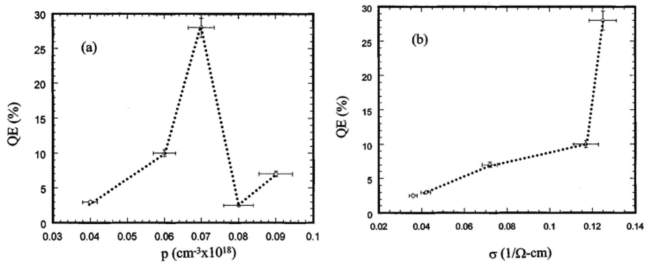

Fig. 1. Quantum efficiency of Cs-activated *p*-GaN photocathodes as a function of (a) hole concentration and (b) *p*-type conductivity. Reprinted from [31] © 2002 IEEE.

Here we will review the progress over the last two decades to achieve high efficiency, stable and high reliability III-nitride photocathodes for detectors applications. Much of this progress focuses on improving the band alignment through band structure and polarization engineering as well as through improvement in *p*-type conductivity by increasing hole concentration and mobility. We will begin by exploring these improvements in *p*-type conductivity in Cs-activated III-nitride photocathodes before discussing novel, air stable Ga- and N-polar GaN structures. Beyond the novel structures, we will describe the iterative improvements in material quality and doping required to achieve photocathodes with high efficiency and lifetime, as well as modeling using Monte Carlo simulations.

II. Cs-Activated Ga-polar GaN Photocathodes

In Cs-activated GaN photocathodes, downward band bending of the semiconductor is needed in addition to the Cs-semiconductor dipole [29]. Downward band bending is achieved with *p*-type doping of III-nitrides and the depletion width is impacted by hole concentration. It should be noted that the magnitude of downward band bending with increasing hole concentration is limited by the pinning of the Fermi level at the surface to the charge neutrality level [30] which is specific to the material properties including polarity and doping type. Increasing hole concentration up to $7x10^{16}$ cm^{-3} in Ga-polar *p*-GaN photocathodes have been shown by Shahedipour *et al.* to increase QE, achieving ~30% efficiency [31]. Further increases in hole concentration result in lowered QE, and there is no continued trend of hole concentration and QE per Fig. 1(a). There is however a clear trend of increasing QE with increasing *p*-type conductivity as shown in Fig. 1(b). Conductivity is the product of the carrier concentration and diffusion length. This result aligns with the theoretical equation of QE given in (3) as the QE has a dependence on both threshold energy and the

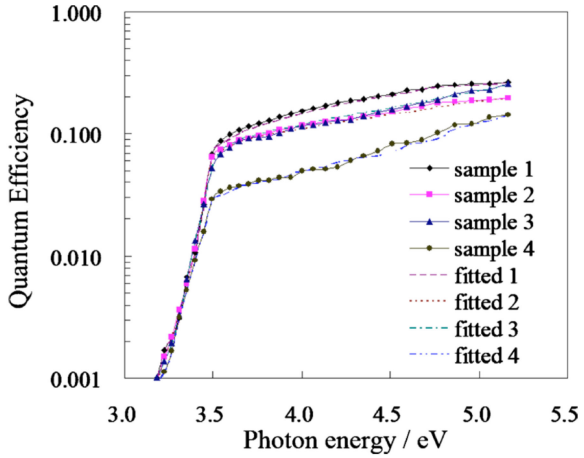

Fig. 2. Quantum efficiency of Ga-polar photocathode samples with varied thickness and *p*-type doping concentration. The hole concentrations were measured to be $1.4x10^{17}$ cm^{-3}, $8.7x10^{16}$ cm^{-3}, $1.6x\ 10^{17}$ cm^{-3}, and $3x10^{18}$ cm^{-3} for Sample 1-4, respectively. Reprinted from X. Wang, *et al.* Appl. Phys. Lett. **98**, 082109 (2011), with the permission of AIP Publishing [35].

electron diffusion length. Increasing hole concentration will decrease E_{th} by minimizing the surface depletion width and lowering the vacuum level relative to the bulk conduction band.

In the III-nitride material system, achieving high hole concentration and large scattering length are often at odds. The relatively large activation energy of the Mg dopant at 160 meV for GaN and increasing with increasing Al content of $Al_xGa_{1-x}N$ [32], leading to a low percentage of activated dopants, typically around 1%. Therefore, a high concentration of Mg atoms must be incorporated in the film to achieve *p*-type conductivity. At high Mg concentrations self-compensation can occur with the formation of V_N [33], and the formation of Mg clusters due to surpassing the solid solubility limit [34]. Studies by Obloh, *et al.* show a parabolic relation of hole concentration with the concentration of incorporated Mg atoms [33]. The authors show increasing hole and Mg concentrations to a maximum point. Further increase in the Mg concentration was shown to lead to decreasing hole concentration, attributed to the formation of V_N. The formation of such defects commonly results in degradation of mobility with increased scattering thereby reducing the electron scattering length. It follows that photocathodes that achieve a high *p*-type conductivity, where conductivity is a measure of both carrier concentration and mobility, result in high QE.

This relationship is further seen in the results of Wang *et al.* of Cs-activated Ga-polar *p*-GaN photocathodes [35]. Low QE was measured for a photocathode with a hole concentration of $3x10^{18}$ cm^{-3}, shown in Fig. 2(sample 4). Fitting of the measured QE to the theoretical equation shows an electron diffusion length in the sample of 43 nm. Comparatively, a QE of 26% at 5.1eV was achieved for a photocathode with $1.4x10^{17}$ cm^{-3} hole concentration (sample 1), and a diffusion length of 122 nm was found via fitting of the data. Many additional studies of III-nitride photocathodes have been reported optimizing [Mg], hole concentration, and conductivity [5], [36], [37]. These results highlight that high hole concentration alone is insufficient to achieve high QE. There must be a balance between hole concentration and mobility to attain both a narrow depletion region and a large electron scattering length. This further shows the importance of achieving high conductivity for enhanced photocathode performance.

Further advancements in Cs-activated GaN photocathodes have produced high QE devices. Through optimization of the [Mg], Uchiyama *et al.* have reported on a photocathode with QE as high as 71.9% at 5.4 eV [5]. Siegmund *et al.* similarly reported up to 70% QE for Cs-activated GaN photocathodes [38]. The Cs-activation used in the previously discussed studies leads to a strong dipole between the Cs and semiconductor, and in conjunction with the downward band bending at the *p*-GaN surface creates effective NEA. The use of Cs also presents numerous challenges, as briefly mentioned above, as it is pyrophoric and reactive to water [39]. The high reactivity leads to the requirement that cesiated photocathodes be activated and maintained in vacuum, increasing the cost of fabrication and deployment. Over time, due to incident high energy radiation or unperfect vacuum the activation decays reducing the efficiency and lifetime of the photocathodes [40]. The susceptibility of the Cs layer to moisture and radiation negates the inherent advantages of III-nitride materials such as radiation-hardness and chemical stability. A thorough review of Cs/Cs-O activated GaN photocathodes, including device design, fabrication and performance has recently been published by Wang *et al.* [41].

III. Cs-free Ga-polar III-nitride Photocathodes

A novel Cs-free photocathode was pioneered by Tripathi *et al.* employing a Si *n*-type delta-doped layer to achieve permanent NEA [42], [43]. The large effective doping of the delta-doped layer assists in lowering the surface conduction band closer to the Fermi-level of the *p*-type bulk layer. This layer must be capped with a highly *n*-type GaN layer to stabilize the surface by preventing oxidation of the delta doped layer. The thickness of the n^+-GaN cap layer is of utmost importance to the photocathode performance. Band diagrams of identical bulk *p*-GaN absorbing and delta-doped layers, with varied thickness of n^+-GaN cap have been simulated by Tripathi *et al.* [42]. The vacuum level relative to the *p*-GaN conduction level decreases with decreasing cap layer thickness, nearing effective NEA with a 3 nm cap, shown in Fig. 3. In this structure, negative fixed charges accumulate at the surface due to polarization discontinuity between the n^+-GaN cap and vacuum.

The effect of cap layer thickness has also been shown experimentally in Fig. 4. Ga-polar *p*-GaN photocathodes with a delta-doped Si layer followed by n^+-GaN cap of thicknesses varied from 2 nm to 11 nm. The photocathode with 2 nm cap resulted in the highest QE of 1.15%. With increasing cap layer thickness, the QE decreases exponentially to a minimum of 0.108% with 11 nm cap. The exponential behavior is well fit to the theoretical dependence of QE on cap thickness and QE attenuation length. The QE attenuation length (L) is dependent on the electron attenuation length (L_e) and photon absorption length (L_{ph}), where $1/L = 1/L_e + 1/L_{ph}$ [42]. The QE attenuation length from fitting the experimental data to this model is 3.45 nm. The absorption length of photons at an energy of

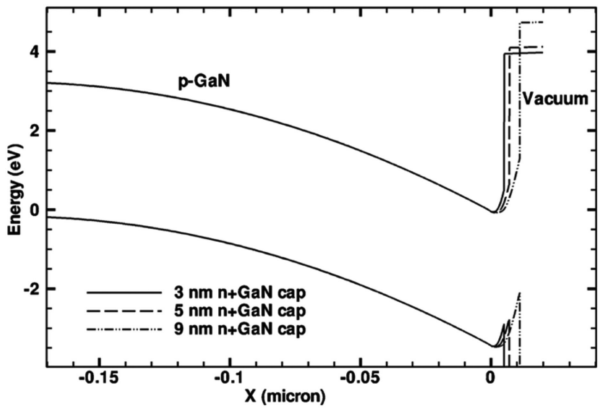

Fig. 3. Simulated energy band diagrams of Cs-free Ga-polar p-GaN photocathodes with n^+GaN cap layer. Reprinted from N. Tripathi, *et al.* Appl. Phys. Lett. **97**, 052107 (2010), with permission of AIP Publishing [42].

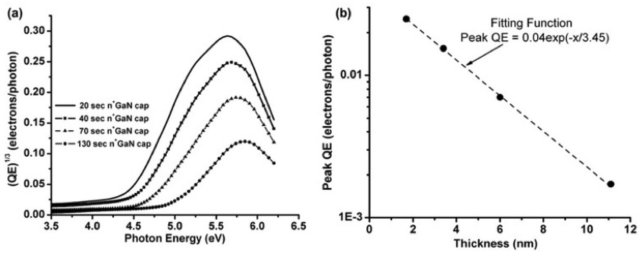

Fig. 4. Experimental photoemission spectra of Ga-polar p-GaN photocathodes with varied n^+-GaN cap layer thickness. Reprinted from N. Tripathi, *et al.* Appl. Phys. Lett. **97**, 052107 (2010), with permission of AIP Publishing [42].

5.5 eV is ∼40 nm, and therefore the QE attenuation length is dominated by the electron diffusion length and not by the photon absorption length. The small diffusion length is due to high carrier scattering resulting from interfacial roughness at the delta-doped/cap interface. As expected, the threshold energy increases with increasing cap layer thickness, shown in the inset of Fig. 4(a). The lowest threshold energy of 4.4 eV is obtained for n^+-GaN cap of 2 nm, corresponding to the highest QE of 1.15%. As expected from the Spicer model and Equation 3, the QE increases non-linearly as a function of threshold energy.

Further studies regarding the Si delta-doping parameters of the novel Cs-free photocathode structure were also reported by Tripathi *et al.* [43]. While a clear trend with photoemission threshold energy was not observed with increasing Si dopant flow rate of the delta-doped layer, increasing roughness, as measured by atomic force microscopy (AFM) was seen. The authors also studied the time of delta-doping at a constant SiH_4 flow of 40 sccm, shown in Fig. 5. The observed decreasing threshold with increasing delta-doping up to 60s is likely the result of increased downward band bending at the surface from the abrupt p-n junction. For a delta-doping time of $>$ 60 s, the threshold energy increases for times of 120 s and 300 s.

The increased threshold energy with increasing delta-doping time beyond 60 s was attributed to increased scattering through examination of the surface microstructure. AFM images of the surface of photocathodes with varied delta-doping time are shown in Fig. 6. The surface roughness increases with increasing

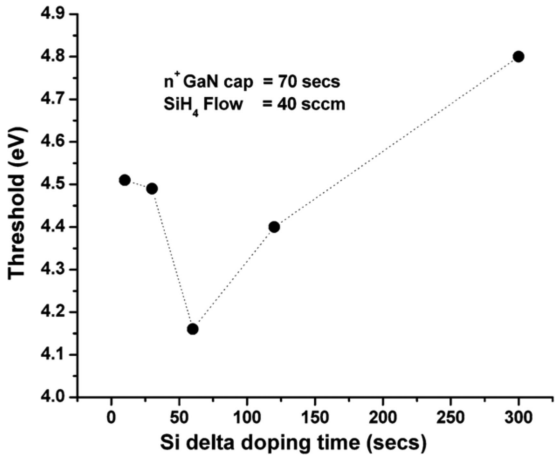

Fig. 5. Threshold energy of Ga-polar photocathodes with varied Si delta doping time. Threshold energy decreases with increasing delta-doping time up to 60 s. Reprinted by permission from Springer Nature, Journal of Electronic Materials, N. Tripathi, *et al.* J. Elec. Mater. 40, 382 (2011). © 2011 [43].

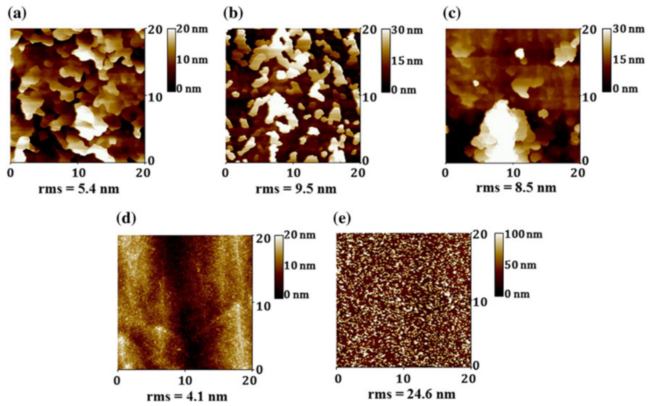

Fig. 6. Atomic force micrographs of delta-doped Ga-polar photocathodes with increasing delta-doping time of (a) 10s, (b) 30 c, (c) 60 s, (d) 120s and (e) 300s. Reprinted by permission from Springer Nature, Journal of Electronic Materials, N. Tripathi, *et al.* J. Elec. Mater. 40, 382 (2011). © 2011 [43].

time up to 60 s, further increases in delta doping time to 120 s results in a smoother surface and the appearance of a different growth mode. Delta-doping for 300s shows a high surface roughness and — on the macro-scale — the formation of large hillocks structures.

A large barrier to further development of Ga-polar Cs-free photocathodes with high quantum efficiency is the presence of intrinsic polarization charge. The use of a n^+-GaN/ p-GaN structure creates a positive depletion charge needed for a large downward band bending in the near surface region. However, in the Ga-polar material the polarization charge is negative at the surface. The polarization compensates the depletion charge and the magnitude of achievable downward band bending is reduced. Increasing electron concentration in the n^+-GaN cap layer is required to overcome the negative polarization charge and increase in the downward band bending. The doping concentrations required to achieve this goal result in low material quality leading to high carrier scattering, shorter electron diffusion length and low QE.

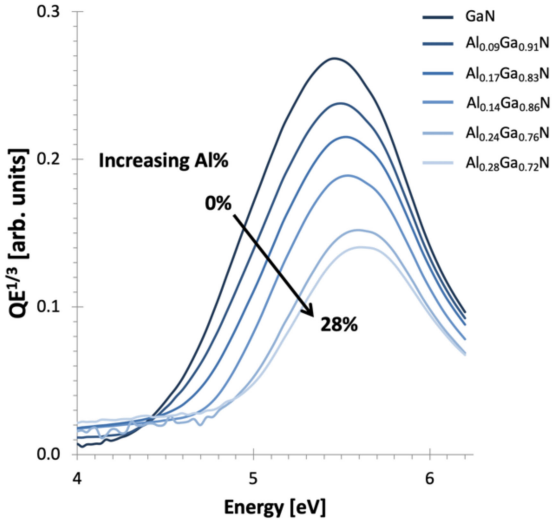

Fig. 7. Photoemission spectra of p-$Al_xGa_{1-x}N$ photocathodes with composition increasing from 0% Al to 28% Al. In general, QE decreases with increasing Al composition due to increasing ionization energy of the Mg dopant in the p-type layer and decreasing material quality.

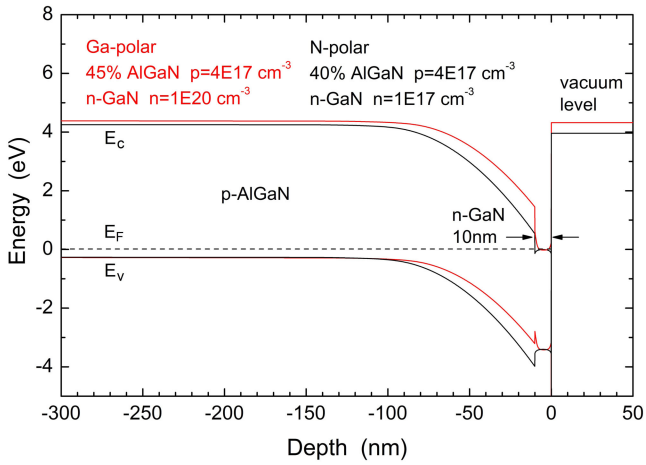

Fig. 8. Energy band diagrams of N-polar (black) and Ga-polar (red) p-AlGaN photocathode structures with n-type GaN cap layers. A depth of 0 nm represents the surface of the photocathode.

In addition to challenges of polarization charge and material quality in Ga-polar GaN photocathodes, $Al_xGa_{1-x}N$ photocathodes targeting UV detection face further obstacles to achieving high QE. Ga-polar p-$Al_xGa_{1-x}N$ photocathodes grown on sapphire substrate by MOCVD show a trend of decreasing maximum QE with increasing Al content varying from 0% to 24%, as in Fig. 7. This is in large part due to the impact of the Mg acceptor activation energy with increasing Al content. As mentioned briefly above, Mg acts as a deep acceptor in GaN 160 meV above the valence band [32], [44]. As Al content increases, the acceptor energy level also increases to 510 meV in AlN [32], [44]. The deep acceptor nature of the Mg dopant leads to decreasing activation efficiency and therefore decreasing hole concentration with increasing Al content. The challenges to achieving high p-type conductivity compounding with compensation from polarization charges have hindered the realization of high QE Ga-polar p-AlGaN photocathodes. Additional challenge is increased surface roughness at higher percentages of Al as measured by AFM.

IV. Cs-free N-polar III-Nitride Photocathodes

While polarization charge in the Ga-polar orientation presents a challenge, in the N-polar orientation it is advantageous. In this orientation the polarization charge at the surface is positive, as well as the heterointerface charge in the case of an AlGaN/GaN heterostructure. The surface-state charge remains positive and the positive polarization charges compound to increase the magnitude of downward band bending at the surface. The impact of the aligned polarization, surface-state and heterointerface charge in the N-polar orientation compared to Ga-polar can be seen through the energy band diagrams of p-AlGaN/n-GaN photocathodes along Ga- and N-polarities shown in Fig. 8. For similar structures, the N-polar photocathode achieved a lower relative surface vacuum level than the Ga-polar. In fact, when grown in the N-polar direction, the photocathode structure is able to use a lower Al composition of the absorbing layer, and a lower n-type doping concentration in the cap layer; both of which allow for improved material quality, and still achieve similar or lower surface vacuum level.

A. Surface Treatments

Initial experiments of N-polar GaN photocathodes, reported by Marini *et al.* did not show the expected improvement in QE predicted by the energy band diagram [45]. For similar p-GaN photocathode structures, the as-grown N-polar device has a measured QE of 2.9% compared to a Ga-polar device with 6.25% QE at 6 eV photon energy. It is well known that N-polar III-nitrides have a thicker native oxide compared to the Ga-polarity [46], [47]. The thicker native oxide on N-polar photocathodes may lead to increased scattering, widening of the potential well at the surface, or unfavorable surface charge and band alignment. Surface oxide can be easily removed through chemical surface cleanings. Many such cleanings have been reported including HCl and $(NH_4)_2S$ solutions [48]. HCl cleaning consisting of 60 s in a 1:10 HCl:ethanol dilution was applied to the N-polar photocathode which resulted in an improvement in device QE to 12% at 6 eV [45]. Conversely, $(NH_4)_2S$ treatment resulted in reduced QE compared to the as-grown photocathode, exhibited in Fig. 9; likely due to unfavorable surface charge reducing the downward surface band bending. Both HCl and $(NH_4)_2S$ treatments resulted in similar removal of oxygen impurities from the surface measured by XPS, decreasing from 3 oxygen monolayers (ML) as-grown, to 1.4 ML and 0.75 ML following HCl and $(NH_4)_2S$ treatments, respectively. Oxide removal using HF was also studied, resulting in similar but slightly less improvement in QE than HCl. The same HCl treatment applied to Ga-polar photocathodes did not result in any noticeable improvement in device QE, which is expected given the lack of significant surface oxide present in the Ga-polarity. The improvement in the N-polar orientation with HCl cleaning is not stable on the order of days when exposed to atmosphere, with QE decaying

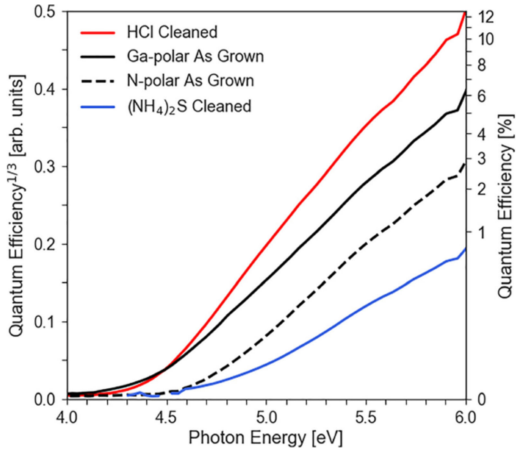

Fig. 9. Photoemission from Ga-polar *p*-GaN photocathode (solid black line), and N-polar photocathodes as-grown (dashed black line), with HCl (red solid line) and $(NH_4)_2S$ (blue solid line) cleanings. Reprinted from J. Marini, *et al.* J. Appl. Phys. **124**, 113101 (2018), with permission of AIP publishing [45].

back to as-grown values. Studies are on-going to achieve an air stable oxide removal and passivation.

In addition to chemical surface treatments, *in situ* surface cleaning via annealing is effective at desorbing contaminants and increasing QE in both Ga- and N-polar photocathodes [49], [50]. Prior to collection of photoemission spectra, QE at a fixed photon energy can be monitored while increasing annealing temperature. From room temperature to 240 °C, little change in photoemission is observed. From 240 – 300 °C the QE increases rapidly. After about 10 minutes at 300 °C, the emission saturates and no further increase is observed. No additional benefit was observed at higher temperatures up to 400 °C. The improved QE following low temperature annealing may be due to desorption of hydrocarbons [49], and/or the emptying of charge from the surface states lowering the effective vacuum level.

B. Impact of N-polar Hillock Structures

Further improvement in N-polar photocathode performance has been achieved by improving the conductivity of the N-polar *p*-GaN film. Studies of Mg dopant incorporation into N-polar GaN by Rocco *et al.* has shown that Mg atoms incorporate more efficiently into the semi-polar facets of hexagonal hillock structures common on the N-polar surface [51]. Atom probe tomography reconstructions of Mg atoms, shown in Fig. 10, from an area in the planar region surrounding a hillock structure show Mg clusters with a density of 5 x 10^{16} cluster/cm^{-3} and a large average radius of 5.1 nm. Comparatively, the Mg incorporation within the hillock semi-polar sidewall is more evenly distributed with a cluster density of 1.8 x 10^{16} cm^{-3} and smaller average radius of 4.8 nm.

The impact of more efficient Mg incorporation into N-polar hillock structures on photocathode performance has been studied by growing photocathode structures of N-polar *p*-GaN and thin *u*-GaN cap layer on high and low hillock density template layers. The density of hexagonal hillock structures can be modified during the growth of N-polar template layers on sapphire by

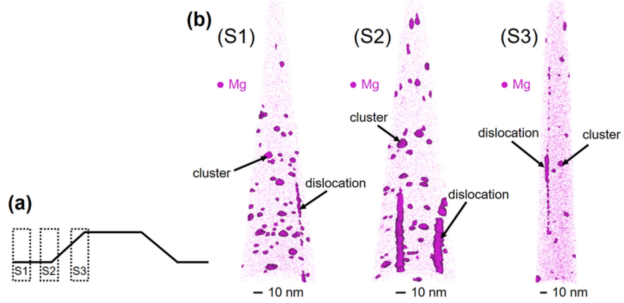

Fig. 10. (a) Schematic of the locations of samples taken across a hillock structure spanning a planar region outside the hillock (S1), at the beginning of the hillock sidewall (S2) and within the hillock semi-polar sidewall (S3), (b) APT reconstructions of Mg atoms from locations spanning a hillock structure. Reprinted from [51], © Rocco, *et al.*

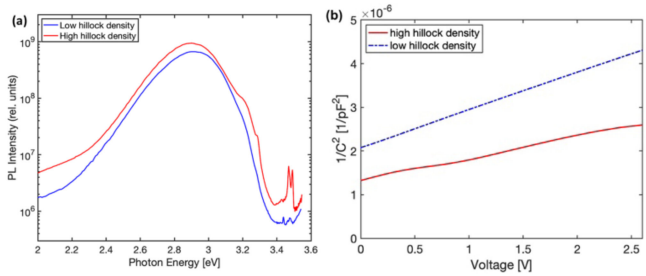

Fig. 11. (a) Low temperature (77 K) photoluminescence spectroscopy and (b) Hg-probe C-V measurement of photocathodes grown on high (red) and low (blue) hillock density N-polar GaN templates. Reprinted from [51], © Rocco, *et al.*

modifying the growth time and utilizing indium surfactant [52]. The photocathode structure grown on high hillock density exhibited improved *p*-type characteristics in photoluminescence measurement, shown in Fig. 11(a), with strong UVL and acceptor bound exciton peaks in addition to a characteristic "blue band" peak observed in heavily Mg-doped films [51]. Further, enhanced *p*-type conductivity of the high hillock density sample is measured by C-V in Fig. 11(b).

The impact of the improved *p*-type conductivity on photocathode emission is seen in photoemission measurements of the same samples. The photocathode grown on high hillock density template achieved a QE of 26.6% at 6 eV photon energy, while the same structure grown on low hillock density template achieved less than half of the former at 10.8% QE, demonstrated in Fig. 12. Interestingly the threshold energy of the photocathode on high hillock density template is higher than on low hillock density template at 4.37 eV and 4.27 eV, respectively. The increase in peak QE without reduction in threshold energy may be due to fewer scattering events as a result of a narrower surface potential well or increased scattering length.

C. Impurity Incorporation in N-polar Photocathodes

Improved conductivity has also been achieved through controlling the unintentional dopant distributions. Oxygen dopants are observed to incorporate more readily in N-polar GaN (compared to Ga-polar) during MOCVD growth due to reduced formation energy of O_N, predicted theoretically [53] and observed

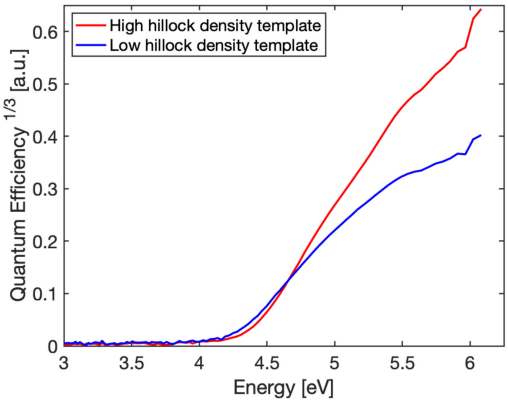

Fig. 12. Photoemission spectra of N-polar *p*-GaN/*u*-GaN cap photocathodes grown on high (red) and low (blue) hillock density *u*-GaN template layers.

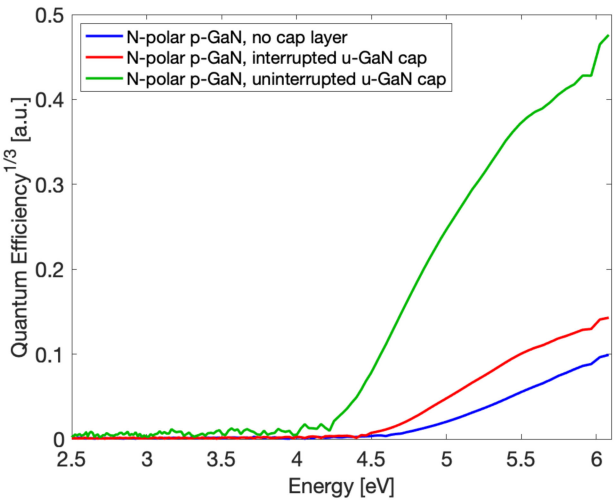

Fig. 13. Photoemission spectra of N-polar *p*-GaN without *u*-GaN cap (blue), with growth interruption prior to *u*-GaN cap (red), and with uninterrupted growth of *p*-GaN/*u*-GaN cap layers (green). Reprinted from E. Rocco, *et al.*, J. Appl. Phys. **129**, 195701 (2021), with permission from AIP Publishing [50].

experimentally [54]. Other unintentional impurities have been observed at regrowth interfaces in a variety of orientations of III-nitrides, most notably silicon [55]–[57]. Unintentional impurities act as scattering centers – and potentially compensating dopants – reducing electron mobility and conductivity and, in turn, photocathode QE.

These effects are seen in the photoemission of N-polar GaN photocathodes consisting of 450 nm *p*-GaN and thin, 10 nm *u*-GaN cap layer with various growth interruption schemes between the bulk *p*-GaN and cap layers, shown in Fig. 13. The bare, N-polar *p*-GaN photocathode with no cap layer achieved a low QE of 0.097%. The addition of a thin *u*-GaN cap layer with growth interruption between the *p*-GaN and cap results in a modestly improved QE to 0.27%. Comparatively, the same structure of *p*-GaN/*u*-GaN cap grown without interruption between layers achieved 10.79% QE.

SIMS measurements on each of the samples revealed spikes in Si and O at all regrowth interfaces [50] with O depth profiles shown in Fig. 14. In each sample there is a spike in O at

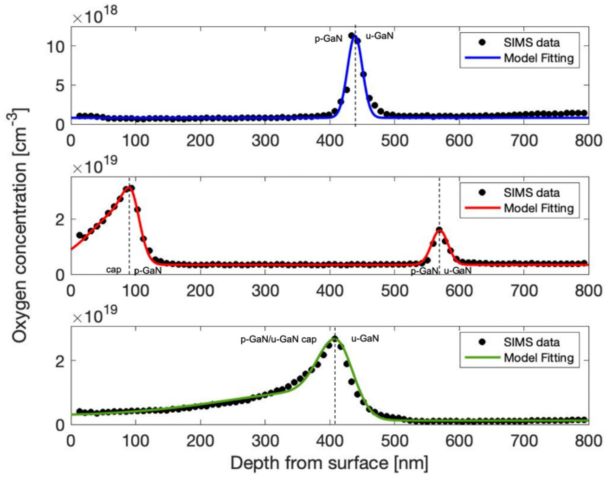

Fig. 14. SIMS depth profiles of oxygen in N-polar *p*-GaN photocathodes with varied growth interruption sequences. (Top) N-polar *p*-GaN (no cap layer), (Middle) Interrupted *u*-GaN cap layer on N-polar *p*-GaN, and (Bottom) Uninterrupted *u*-GaN cap on N-polar *p*-GaN. The surface is at 0 nm depth with increasing depth into the bulk of the sample. Data from [50].

the interface between the N-polar *u*-GaN template layer and the bulk *p*-GaN absorbing layer. The lower photoemission of the interrupted cap layer photocathode has been attributed to the additional spike in oxygen and silicon concentration between the *p*-GaN and cap layers, leading to increased scattering and altering the intended electrostatic profile (Fig. 14, middle). The uninterrupted *p*-GaN/*u*-GaN cap photocathode exhibits only the singular regrowth interface between the template and *p*-GaN layers. The profile of oxygen concentration shows a broad exponential decay from that interface spike towards the surface (Fig. 14, bottom). This behavior is indicative of a pipe diffusion of oxygen through dislocations.

Oxygen diffusion in each photocathode was modeled based on the [O] profile measured by SIMS. A bulk diffusion of oxygen was observed at the template/ *p*-GaN interface of the no-cap photocathode. In the uninterrupted cap photocathode combined bulk and pipe diffusion is well fit to the oxygen depth profile. Dislocation-mediated pipe diffusion allows for a high diffusivity of the species and allows for oxygen to diffuse to a greater depth [58]. In this case an elevated oxygen concentration is observed throughout the near surface region. In comparison to the high [O] concentration in the surface region of interrupted cap sample which is likely to negatively impact the intended electrostatic profile, the moderate oxygen concentration in the uninterrupted cap sample at a Mg:O ratio of 4:1 may allow for co-doping of Mg and O [50]. Mg co-doping with O has been shown to decrease the acceptor activation energy leading to higher hole concentrations [59]. Additionally, Mg-O ion pairs act as dipole scattering centers which have a lower scattering rate than coulombic scattering centers [60]. These impacts of co-doping may improve the conductivity in the *p*-type photocathode layer in the near surface region yielding higher QE. These results highlight the importance of control and engineering of the electrostatic profile within photocathode structures.

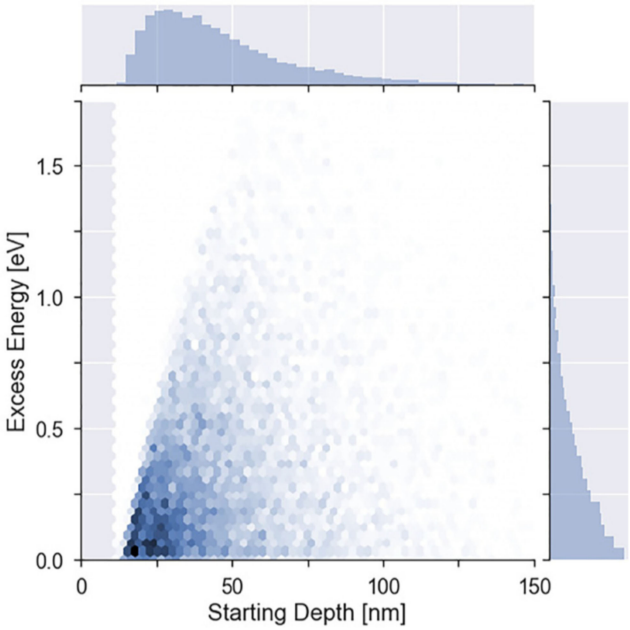

Fig. 15. Heat map distribution of emitted electrons as a function of photoexcitation depth (on x-axis) and excess energy above the vacuum level (on y-axis). The darkness of the color indicates increasing density of points. Reprinted from J. Marini, L.D. Bell, F. Shahedipour-Sandvik, J. Appl. Phys. **123**, 124502 (2018), with permission of AIP publishing [61].

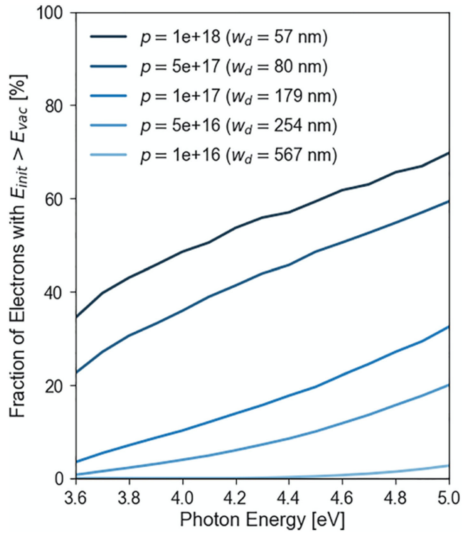

Fig. 16. Simulated fraction of excited electrons with sufficient energy for photoemission at varied hole concentrations (surface depletion widths). Reprinted from J. Marini, *et al.* J. Appl. Phys. **124**, 113101 (2018), with permission of AIP publishing [45].

V. Monte Carlo Simulations of Photocathodes

The importance of the electrostatic profile in the near surface region has been reported theoretically by Marini *et al.* [61]. The Monte Carlo simulation package Archimedes was adapted to include functionality with nitride semiconductors, 3-valley materials, as well as to add photoexcitation and emission models, and scattering mechanisms relevant to minority carrier transport. Through Monte Carlo simulations individual electrons are tracked spatially and energetically from the initial time of photoexcitation. From this capability, the starting depth of electrons that are ultimately emitted can be examined as well as the excess energy of these electrons at the time of emission, as shown in Fig. 15. Here, excess energy is defined as energy above the vacuum level at the time of emission. The majority of emitted electrons have initial photoexcitation within 70 nm of the surface [61]. In this structure 70 nm corresponds to the edge of the depletion region. Further, the majority of electrons are emitted with little excess energy. These results, while expected, underscores the need for control of the electrostatic profile in the near surface region to obtain sharp downward band bending with a narrow surface potential well, and to maintain high conductivity of the material to minimize scattering events.

Monte Carlo simulation of Ga-polar *p*-GaN photocathode structures have also been used to simulate the importance of high hole concentration and the magnitude of downward surface band bending. Increased hole concentration narrows the width of the surface depletion region or potential well. Electrons excited outside of the potential well require energy greater than the effective electron affinity to escape into vacuum. Carriers excited within the well or that thermalize to the conduction band minimum within the potential well require increased energy to escape. We see this result in Fig. 16 showing the impact of varied hole concentration (and depletion width) on the fraction of photoexcited electrons with initial energy above the vacuum level in Ga-polar *p*-GaN photocathodes. Here, a larger percentage of electrons are excited with sufficient energy to escape the surface as the hole concentration increases. These simulations do not account for changes in *p*-type conductivity, which may impact transport, specifically at high Mg concentrations where self-compensation is common, as discussed above. An ideal photocathode structure has high hole concentration to achieve a desired electrostatic profile and high mobility, as discussed previously with Cs-activated Ga-polar *p*-GaN photocathodes Fig. 1(b), in order to minimize scattering of photoexcited electrons that may lower the carrier energy with respect to the vacuum level.

These Monte Carlo simulations also highlight the significance of maximizing the magnitude of downward surface band bending. Fig. 17 shows Ga-polar *p*-GaN photocathodes that were simulated with varied downward surface band bending and constant hole concentration of 10^{17} cm^{-3}. Quantum efficiency increases with larger downward band bending, as expected. In experiment such large magnitudes of band bending is difficult to achieve due to pining of the fermi-level due to surface states [30], [62] as a result of terminating the periodic crystal and, in part, due to the chemical state of the surface. Cleaning of the surface is of importance to maximize the possible downward surface band bending, as discussed with the initial N-polar GaN studies of surface cleaning, which in turn will lower vacuum level relative to the bulk conduction level.

Beyond predicative modeling of photocathode performance, the addition of satellite valley transport within the Monte Carlo simulations developed by Marini *et al.* provides insight into fundamental GaN material parameters such as effective mass in upper valleys and energy offset between the Γ_1 and upper valleys. The band structure parameters in the Γ_1 valley are largely

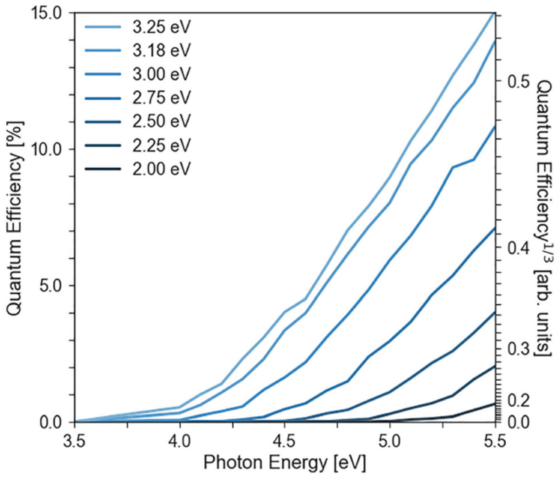

Fig. 17. Simulated Ga-polar *p*-GaN photocathode (10^{17} cm^{-3} hole concentration) with the magnitude of downward band bending varied from 2.00 eV to 3.25 eV. Reprinted from J. Marini, *et al.* J. Appl. Phys. **124**, 113101 (2018), with permission of AIP publishing [45].

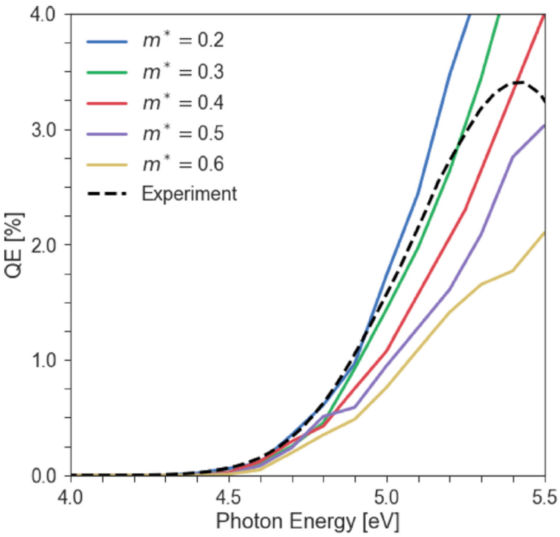

Fig. 18. Monte Carlo simulation of Ga-polar *p*-GaN (hole concentration 10^{17} cm^{-3}) photocathodes with varied values for the effective mass in the M-L valley in solid colored lines compared to experimental results in black dashed line. Reprinted from J. Marini, L.D. Bell, F. Shahedipour-Sandvik, J. Appl. Phys. **123**, 124502 (2018), with permission of AIP publishing [61].

in agreement across literature with an effect mass, $m^* = 0.2m_0$. Many studies utilize an effective mass in the upper M-L valley of $1.0m_0$ while theoretical calculations of the band parameters in the upper M-L valley suggest an effective mass of $0.4m_0$. [63]. Monte Carlo simulations of a Ga-polar *p*-GaN photocathode with varied electron effective mass in the M-L valley from $0.2m_0$ to $0.6m_0$ were compared to experimental photoemission results shown in Fig. 18. Varying effective mass in the M-L valley results in significant differences between photoemission slope, indicating that transport in the upper valley is significant, as transport in the primary Γ_1 valley is minimally impacted by the effective mass of the upper valleys. An effective mass of $m^* = 0.3m_0$ used in simulating the photoemission yields the closest match with experiment. Further experimentation and simulation should be used both for accurate photocathode simulation and for band structure parameters used broadly in the field.

VI. Comparison of Cs-Activated and Cs-Free GaN Photocathodes

GaN photocathodes activated with Cs or Cs/O have some advantages in terms of maximum achievable QE and threshold energy compared to the current state of the art Cs-free GaN photocathodes. As previously mentioned in Section I, the Cs or Cs/O layer creates a dipole barrier at the surface and lowers the vacuum energy relative to GaN conduction band creating effective NEA. A large fraction of photoexcited carriers reaching the surface will successfully tunnel through the barrier and be emitted into vacuum. This enables the high QEs above 70% that have been reported [5], [38]. While the Cs-free photocathode structures have been engineered to target NEA conditions by lowering the vacuum level at the surface without a dipole tunneling barrier, it is unlikely that these structures have achieved a true NEA condition.

Cs-activation also impacts device threshold energy. Many Cs-activated photocathodes have a sharp threshold energy at or near the bandgap energy. With the NEA condition induced by the Cs dipole, all photoexcited carriers have a probability for photoemission. In a Cs-free device, if the structure has not achieved NEA a photoexcited electron is required to have an additional amount of energy beyond the bandgap to be emitted. As a result, many Cs-free III-nitride photocathodes exhibit threshold energies above the bandgap. These qualities in both Cs-activated and Cs-free photocathodes can be utilized to tune the cut-off energy. For example, in the case of devices targeting mid- to far-UV energies, larger threshold energy without the need for high composition alloying (and thus the challenges of obtaining high p-type conductivity AlGaN films) may be advantageous.

A distinct advantage of Cs-free photocathodes lies in the stability of the structure. Cs and Cs/O surface activation is unstable in the presence of many gases, most notably H_2O, CO, CO_2, and CH_4 resulting in decreased QE [64]. There remains debate on the stability of the activation layer in N_2 ambient [13], [38], [64]. The QE can be recovered to some degree by annealing after exposure to desorb CO and CO_2 and recovered fully by redepositing the Cs/O activation layer [13].

Ga-polar Cs-free photocathodes do not require surface pretreatment prior to measurement. Once inside the measurement chamber an anneal at 300 °C is used to desorb surface contaminants prior to measurement. Under constant illumination on the order of days, QE of these devices is seen to decrease possibly due to accumulation of charge at the surface. However, when the light is turned off, no measurable decay in QE is observed with similar values prior to and following the sample sitting in the dark for a number of days. Similar experimentation of Cs-activated GaN photocathodes show a decay in QE even when kept in the dark between measurements [65]. N-polar GaN photocathodes have additional decay even when kept in the dark, possibly due to differences in surface states or oxidation due to imperfect vacuum.

The improved stability of Cs-free photocathodes provides a number of advantages. First, the devices have a long lifetime once in vacuum. The devices will not require frequent changing of samples for applications such as electron sources for accelerators where it is inconvenient, or space applications where it is impossible to exchange devices. Further, Cs-free devices simplify measurement and operational set-ups, removing the need for an *in-situ* Cs source or transport in vacuum for cesiated devices.

VII. Conclusion and Outlook

Significant advancements toward high efficiency, air-stable Cs-free III-nitride photocathodes over the last two decades have employed novel band structure, polarization and surface engineering techniques. The experimental and theoretical studies discussed in this review emphasize the imperative to control the electrostatic profile of photocathode devices. High p-type conductivity and surface state have been shown to be important factors impacting the electrostatic profile and QE.

Increased hole concentration is advantageous in III-nitride photocathodes leading to a decreased width of the surface potential well. High p-type conductivity films in N-polar p-GaN photocathodes have been achieved through improved incorporation efficiency in semi-polar planes of hillock structures, resulting in 26% QE. Further, the electrostatic profile and p-type conductivity can be improved by controlling unintentional impurity incorporation and diffusion throughout the device. Beyond improvement in the electrostatic profile, improvements in p-type conductivity may also have some benefit through increasing the scattering length of electrons.

Surface cleaning has also been studied through *ex situ* wet chemical treatments and *in situ* annealing. An order of magnitude improvement in QE has been shown after HCl cleaning of N-polar GaN photocathodes, due to the removal of surface oxide and the creation of favorable surface charge. Additionally, *in situ* annealing desorbs contaminants and/or modification of surface states.

In order for Cs-free GaN devices to achieve their full potential as robust, high efficiency, stable photocathodes the following pathways are proposed:

A. Further Improvement in QE By the Use of Novel Device Structures and Improvements in Material Quality

In order to realize the highest possible QE an NEA or effective NEA condition must be met. One possibility for a novel device structure to achieve this is the addition of an AlN interlayer between N-polar p-$Al_xGa_{1-x}N$ and n-GaN cap layer which has been shown in simulation to create a quasi-band offset and improve NEA [45]. In this structure the depletion width may be reduced with the addition of polarization charge at the p-AlGaN/AlN interface supplementing the depletion charge in p-AlGaN layer. The AlN interlayer may act as a tunneling barrier similar to what is obtained with Cs/O activation, and provide an air-stable realization of NEA. The material quality of Cs-free photocathodes must also be improved to achieve the highest possible QE. Increased hole concentration has been achieved in the Ga-polarity with Mg delta-doping leading to increased QE [37]. Unfortunately, similar methodology was not successful for the N-polarity of III-nitrides [66]. Further novel doping techniques building off the results of increased Mg incorporation efficiency in N-polar hillock structures should be explored to increase the p-type conductivity of photocathodes layers.

B. Development of Surface Passivation Techniques for N-polar III-nitride Material

Further experimentation of wet chemical processes should be completed in search of a stable treatment which leads to the removal of surface oxide and contaminants, while creating favorable surface charge. Novel surface coatings for GaN photocathodes should also be explored. Liu *et al.* recently proposed the use of Al nanoparticles deposited on the surface of GaN photocathodes for improved QE [67]. Atomically thin coatings that may increase light absorption, create favorable surface charge and prevent surface contamination may provide a path toward high QE, highly stable photocathodes.

The achievement of high efficiency, air-stable III-nitride photocathodes will benefit a range of disciplines. High reliability, long lifetime single photon detectors can be employed in astronomy and military applications. Advances in lifetime and energy distribution of emitted electrons may also assist applications in high-brightness electron sources. Given the wide range of applications for photocathodes, a tailored approach toward device design and implementation may be required to optimize devices for specific purposes.

Acknowledgment

This research was carried out in part at the Jet Propulsion Laboratory, California Institute of Technology.

References

[1] E. Muñoz, E. Monroy, J. L. Pau, F. Calle, F. Omnès, and P. Gibart, "III nitrides and UV detection," *J. Phys. Condens. Matter*, vol. 13, no. 32, 2001, Art. no. 7115.

[2] C. Rivera, J. Pereiro, A. Navarro, E. Muñoz, O. Brandt, and H. T. Grahn, "Advances in Group-III-Nitride photodetectors," *Open Electr. Electron. Eng. J.*, vol. 4, pp. 1–9, 2010.

[3] B. Alshehri *et al.*, "Dynamic characterization of III-Nitride-based high-speed photodiodes," *IEEE Photon. J*, vol. 9, no. 4, Aug. 2017, Art. no. 6803107, doi: 10.1109/jphot.2017.2714168.

[4] S. Donati and T. Tambosso, "Single-photon detectors: From traditional PMT to solid-state SPAD-based technology," *IEEE J. Sel. Top. Quantum Electron.*, vol. 20, no. 6, pp. 204–211, Nov./Dec. 2014.

[5] S. Uchiyama, Y. Takagi, M. Niigaki, H. Kan, and H. Kondoh, "GaN-based photocathodes with extremely high quantum efficiency," *Appl. Phys. Lett.*, vol. 86, no. 10, Mar. 2005, Art. no. 103511, doi: 10.1063/1.1883707.

[6] P. Suvarna *et al.*, "Design and growth of visible-blind and solar-blind III-N APDs on sapphire substates," *J. Electron. Mater.*, vol. 42, no. 5, pp. 854, 2013, doi: 10.1007/s11664-013-2537-8.

[7] J. Xie *et al.*, "Large area planar photocathode for MCP-based photodetectors," *Nucl. Instrum. Methods Phys. Res. A*, vol. 955, 2020, Art. no. 163234.

[8] X. Xu and J. Guo, "New EBCCD with transferred electron photocathode for range-gated active imaging system," in *Proc. SPIE Adv. Mater. Devices Sens. Imag.*, vol. 4919, 2002, pp. 536–544.

[9] P. Townsend, "Photocathode—past performance and future potential," *Contemp. Phys.*, vol. 44, no. 1, pp. 17–34, 2003, doi: 10.1080/00107510302717.

[10] I. V. Bazarov, L. Cultrera, and T. Rao, "Semiconductor photocathodes for unpolarized electron beams," in *Proc. An Eng. Guide to Photoinjectors*, 2013, pp. 184–217.

[11] H. Lee, S. Karkare, L. Cultrera, A. Kim, and I. V. Bazarov, "Review and demonstration of ultra-low-emittance photocathode measurements," *Rev. Sci. Instrum.*, vol. 86, 2015, Art. no. 073309.

[12] I. V. Bazarov *et al.*, "Thermal emittance and response time measurements of a GaN photocathode," *J. Appl. Phys.*, vol. 105, 2009, Art. no. 083715, doi: 10.1063/1.3110075.

[13] D. Sato, T. Nishitani, Y. Honda, and H. Amano, "Recovery of quantum efficiency on Cs/O-activated GaN and GaAs photocathodes by thermal annealing in vacuum," *J. Vac. Sci. Technol. B*, vol. 38, 2020, Art. no. 012603, doi: 10.1116/1.5120417.

[14] W. E. Spicer and A. Herrera-Gomez, "Modern theory and applications of photocathodes," in *Proc. Photodetectors Power Meters*, Oct. 1993, vol. 2022, pp. 18–36. doi: 10.1117/12.158575.

[15] W. E. Spicer, "Photoemissive, photoconductive, and optical absorption studies of alkali-antimony compounds," *Phys. Rev.*, vol. 112, no. 1, pp. 114–122, 1958.

[16] V. M. Shalaev, "Electron escape and photoemission in the threshold region," *Phys. Rev. B*, vol. 49, no. 2, 1994, Art. no. 1437, doi: 10.1103/PhysRevB.49.1437.

[17] R. J. Powell, "Interface barrier energy determination from voltage dependence of photoinjected currents," *J. Appl. Phys.*, vol. 41, 1970, Art. no. 2424, doi: 10.1063/1.1659238.

[18] I.-S. Chen, T. N. Jackson, and C. R. Wronski, "Characterization of semiconductor heterojunctions using internal photoemission," *J. Appl. Phys.*, vol. 79, 1996, Art. no. 8470, doi: 10.1063/1.362522.

[19] T. Norton, B. Woodgate, J. Stock, G. Hilton, and M. Ulmer, "Results from Cs activated GaN photocathode development for MCP detector systems at NASA GSFC," in *Proc. SPIE Opt. Sci. Technol.*, San Diego, CA, 2003, Art. no. 5164, doi: 10.1117/12.507528.

[20] V. Jhalani, J.-J. Zhou, and M. Bernardi, "Ultrafast hot carrier dynamics in GaN and its impact on the efficiency droop," *Nano Lett*, vol. 17, 2017, Art. no. 5012, doi: 10.1021/acs.nanolett.7b02212.

[21] A. Ganose, J. Park, A. Faghaninia, R. Woods-Robinson, K. Persson, and A. Jain, "Efficient calculations of carrier scattering rates from first principles," *Nat. Commun.*, vol. 12, 2021, Art. no. 2222, doi: 10.1038/s41467-021-22440-5.

[22] A. Lorusso, "Overview and development of metallic photocathodes prepared by laser ablation," *Appl. Phys. A*, vol. 110, pp. 869–875, 2013.

[23] O. H. W. Siegmund, E. Everman, J. V. Vallerga, J. Sokolowski, and M. Lampton, "Ultraviolet quantum detection efficiency of potassium bromide as an opaque photocathode applied to microchannel plates," *Appl. Opt.*, vol. 26, no. 17, 1987, Art. no. 3607, doi: 10.1364/AO.26.003607.

[24] O. H. W. Siegmund, J. McPhate, T. Curtis, J. V. Jelinksky, J. Hull, and J. Tedesco, "Ultraviolet imaging detectors for the GOLD mission," in *Proc. Space Telescopes Instrum.: Ultraviolet to Gamma Ray*, Edinburgh, U.K., 2016, Art. no. 99050D. doi: 10.1117/12.2232219.

[25] C. Sinclair, "Very high voltage photoemission electron guns," presented at the Particle Accelerator Conference, 2003. Accessed: Jun. 3, 2021. [Online]. Available: https://accelconf.web.cern.ch/p03/papers/mopb006.pdf

[26] L. Cultrera, J. Maxson, and I. Bazarov, "Photocathode behavior during high current running in the Cornell energy recovery linac photoinjector," *Phys. Rev. Spec. Top. - Accel. Beams*, vol. 16, 2013, Art. no. 021301. http://dx.doi.org/10.1103/PhysRevSTAB.16.021301.

[27] Y. Zhang *et al.*, "High-efficiency graded band-gap AlxGa1-xAs/GaAs photocathodes grown by metalorganic chemical vapor deposition," *Appl. Phys. Lett.*, vol. 99, 2011, Art. no. 101104, doi: 10.1063/1.3635401.

[28] G. Hao, M. Yang, B. Chang, X. Chen, J. Zhang, and X. Fu, "Attenuation performance of reflection-mod AlGaN photocathode under different preparation methods," *Appl. Opt.*, vol. 52, no. 23, 2013, Art. no. 5671, doi: 10.1364/AO.52.005671.

[29] M. Eyckeler and W. Mönch, "Negative electron affinity of cesiated p-GaN (0001) surfaces," *J. Vac. Sci. Technol. B*, vol. 16, 1998, Art. no. 2224.

[30] P. Reddy *et al.*, "The effect of polarity and surface states on the Fermi level at III-nitride surfaces," *J. Appl. Phys.*, vol. 116, 2014, Art. no. 123701.

[31] F. Shahedipour, M. P. Ulmer, B. W. Wessels, C. L. Joseph, and T. Nihashi, "Efficient GaN photocathode for low-level ultraviolet signal detection," *IEEE J. Quantum Electron.*, vol. 38, no. 4, pp. 333–335, Apr. 2002, doi: 10.1109/3.992544.

[32] M. Katsuragawa *et al.*, "Thermal ionization energy of Si and Mg in AlGaN," *J. Cryst. Growth*, vol. 189, pp. 528, 1998, doi: 10.1016/S0022-0248(98)00345-5.

[33] H. Obloh *et al.*, "Self-compensation in Mg doped p-type GaN grown by MOCVD," *J. Cryst. Growth*, vol. 195, no. 1, pp. 270–273, Dec. 1998, doi: 10.1016/S0022-0248(98)00578-8.

[34] S. Khromov *et al.*, "Atom probe tomography study of Mg-doped GaN layers," *Nanotechnology*, vol. 25, 2014, Art. no. 275701.

[35] X. Wang, B. Chang, L. Ren, and P. Gao, "Influence of the p-type doping concentration on reflection-mode GaN photocathode," *Appl. Phys. Lett.*, vol. 98, 2011, Art. no. 082109, doi: 10.1063/1.3556656.

[36] X. Zhang, B. Cao, and X. Wang, "Theoretical optimization of the hole concentration for GaN photocathode," *Opt. Mater.*, vol. 84, pp. 586–592, Oct. 2018, doi: 10.1016/j.optmat.2018.07.056.

[37] X. Wang and Y. Zhang, "Negative electron affinity GaN photocathode with Mg delta-doping," *Optik*, vol. 168, pp. 278–281, 2018, doi: 10.1016/j.ijleo.2018.04.112.

[38] O. Siegmund *et al.*, "Development of GaN photocathodes for UV detectors," *Nucl. Instrum. Methods Phys. Res. A*, vol. 567, pp. 89–92, 2006.

[39] W. C. Butterman, W. E. Brooks, and R. G. Reese, Jr, "Mineral commodity profiles: Cesium," USGS, USA, Report 2004–1432, 2005. doi: 10.3133/ofr20041432.

[40] A. S. Tremsin and O. H. W. Siegmund, "The quantum efficiency and stability of UV and soft X-ray photocathodes," in *Proc. Ultrafast X-Ray Detectors, High-Speed Imag., Appl.*, Sep. 2005, vol. 5920, Art. no. 59200I. doi: 10.1117/12.621761.

[41] X. Wang *et al.*, "Negative electron affinity of the GaN photocathode: A review on the basic theory, structure design, fabrication, and performance characterization," *J. Mater. Chem. C*, vol. 9, 2021, Art. no. 13013, doi: 10.1039/d1tc03244e.

[42] N. Tripathi, L. D. Bell, S. Nikzad, and F. Shahedipour-Sandvik, "Effect of n+GaN cap polarization field on Cs-free GaN photocathode characteristics," *Appl. Phys. Lett.*, vol. 97, no. 5, Aug. 2010, Art. no. 052107, doi: 10.1063/1.3476341.

[43] N. Tripathi, L. D. Bell, S. Nikzad, M. Tungare, P. H. Suvarna, and F. Shahedipour-Sandvik, "Novel Cs-free GaN photocathodes," *J. Electron. Mater.*, vol. 40, no. 4, pp. 382, 2011.

[44] B. N. Pantha, J. Y. Lin, and H. X. Jiang, "High-Quality Al-Rich AlGaN alloys," in *GaN and ZnO-based Materials and Devices*, S. Pearton, Ed., vol. 156, Berlin Heidelberg, Germany: Springer, 2012, pp. 29–81.

[45] J. Marini, I. Mahaboob, E. Rocco, L. D. Bell, and F. Shahedipour-Sandvik, "Polarization engineered N-polar Cs-free GaN photocathodes," *J. Appl. Phys.*, vol. 124, no. 11, Sep. 2018, Art. no. 113101, doi: 10.1063/1.5029975.

[46] J. Ferguson, "Investigation of surface properties for Ga- and N-polar GaN using scanning probe microscopy techniques," Ph.D. dissertation, Virginia Commonwealth Univ., Richmond, VA, USA, 2013.

[47] S. Choi *et al.*, "Band bending and adsorption/desorption kinetics on N-polar GaN surfaces," *J. Vac. Sci. Technol. B Microelectron. Nanometer Struct. Process. Meas. Phenom.*, vol. 27, no. 1, pp. 107–112, Jan. 2009, doi: 10.1116/1.3054345.

[48] G. L. Martinez, M. R. Curiel, B. J. Skromme, and R. J. Molnar, "Surface recombination and sulfide passivation of GaN," *J. Electron. Mater.*, vol. 29, no. 3, pp. 325–331, doi: 10.1007/s11664-000-0072-x.

[49] O. E. Tereshchenko *et al.*, "Low-temperature method of cleaning p-GaN (0001) surfaces for photoemitters with effective negative electron affinity," *Phys. Solid State*, vol. 46, pp. 1949–1953, 2004.

[50] E. Rocco *et al.*, "Impurity incorporation and diffusion from regrowth interfaces in N-polar GaN photocathodes and the impact on quantum efficiency," *J. Appl. Phys.*, vol. 129, no. 19, 2021, Art. no. 195701.

[51] E. Rocco *et al.*, "Hillock assisted p-type enhancement in N-polar GaN:Mg films grown by MOCVD," *Sci. Rep.*, vol. 10, no. 1, pp. 1–8, Jan. 2020, doi: 10.1038/s41598-020-58275-1.

[52] J. Marini, J. Leathersich, I. Mahaboob, J. Bulmer, N. Newman, and F. Shahedipour-Sandvik, "MOCVD growth of N-polar GaN on on-axis sapphire substrate: Impact of AlN nucleation layer of GaN surface hillock density," *J. Cryst. Growth*, vol. 442, pp. 25–30, 2016.

[53] T. Zywietz, J. Neugebauer, and M. Scheffler, "The adsorption of oxygen at GaN surfaces," *Appl. Phys. Lett.*, vol. 74, no. 12, 1999, Art. no. 1695, doi: 10.1063/1.123658.

[54] N. A. Fitchenbaum, T. E. Mates, S. Keller, S. P. DenBaars, and U. K. Mishra, "Impurity incorporation in heteroepitaxial N-face and Ga-face GaN fims grown by metalorganic chemical vapor deposition," *J. Cryst. Growth*, vol. 310, no. 6, pp. 1124–1131, 2008, doi: 10.1016/j.jcrysgro.2007.12.051.

[55] M. Monavarian *et al.*, "High-voltage rEgrown nonpolar m-Plane vertical p-n diodes: A step toward future selective-area-doped power switches," *IEEE Electron Device Lett*, vol. 40, no. 3, pp. 387–390, Mar. 2019, doi: 10.1109/LED.2019.2892345.

[56] A. Aragon *et al.*, "Interfacial impurities and their electronic signatures in high-voltage regrown nonpolar m-Plane GaN vertical p–n diodes," *Phys. Status Solidi A*, vol. 217, no. 7, 2020, Art. no. 1900757, doi: 10.1002/pssa.201900757.

[57] K. Fu *et al.*, "Investigation of GaN-on-GaN vertical p-n diode with regrown p-GaN by metalorganic chemical vapor deposition," *Appl. Phys. Lett.*, vol. 113, no. 23, 2018, Art. no. 233502, doi: 10.1063/1.5052479.

[58] S. J. Pearton, H. Cho, J. R. LaRoche, F. Ren, R. G. Wilson, and J. W. Lee, "Oxygen diffusion into SiO_2-capped GaN during annealing," *Appl. Phys. Lett.*, vol. 75, no. 19, pp. 2939–2941, Nov. 1999, doi: 10.1063/1.125194.

[59] R. Y. Korotkov, J. M. Gregie, and B. W. Wessels, "Electrical properties of p-type GaN:Mg codoped with oxygen," *Appl. Phys. Lett.*, vol. 78, no. 2, pp. 222–224, Jan. 2001, doi: 10.1063/1.1335542.

[60] K. H. Ploog and O. Brandt, "Doping of group III nitrides," *J. Vac. Sci. Technol. Vac. Surf. Films*, vol. 16, 1998, Art. no. 1609, doi: 10.1116/1.581128.

[61] J. Marini, L. D. Bell, and F. Shahedipour-Sandvik, "Monte Carlo simulation of III-nitride photocathodes," *J. Appl. Phys.*, vol. 123, no. 12, Mar. 2018, Art. no. 124502, doi: 10.1063/1.5022200.

[62] V. M. Bermudez, "The fundamental surface science of wurtzite gallium nitride," *Surf. Sci. Rep.*, vol. 72, pp. 147–315, 2017.

[63] U. V. Bhapkar and M. S. Shur, "Monte Carlo calculation of velocity-field characteristics of wurtzite GaN," *J. Appl. Phys.*, vol. 82, no. 4, 1997, Art. no. 1649, doi: 10.1063/1.365963.

[64] F. Lu, L. Liu, and J. Tian, "Residual gas adsorption effect on the stability of Cs-activated GaN nanowire photocathode," *Appl. Surf. Sci.*, vol. 497, 2019, Art. no. 143791, doi: 10.1016/j.apsusc.2019.143791.

[65] T. Nishitani, M. Tabuchi, H. Amano, T. Maekawa, M. Kuwahara, and T. Meguro, "Photoemission lifetime of a negative electron affinity gallium nitride photocathode," *J. Vac. Sci. Technol. B*, vol. 32, 2014, Art. no. 06F901. [Online]. Available: https://avs.scitation.org/doi/10.1116/1.4901566

[66] J. Marini, I. Mahaboob, K. Hogan, S. Novak, L. D. Bell, and F. Shahedipour-Sandvik, "Mg incorporation efficiency in pulsed MOCVD of N-Polar GaN:Mg," *J. Electron. Mater.*, vol. 46, no. 10, pp. 5820–5826, Oct. 2017, doi: 10.1007/s11664-017-5602-x.

[67] L. Liu, X. Zhangyang, Z. Lv, F. Lu, and J. Tian, "Enhanced light trapping in GaN thin films with al nanoparticles for photocathode applications," *Mater. Sci. Eng. B*, vol. 269, 2021, Art. no. 115158.